

## Iron Nitride Catalysts For Synthesis Reactions

W.N. Delgass, A.A. Hummel, A.P. Wilson, and K.E. Hummel

School of Chemical Engineering  
Purdue University  
West Lafayette, Indiana 47907

### INTRODUCTION

Synthesis gas (CO and H<sub>2</sub>) from coal is a potential source of both fuels and chemical feedstocks. Commercial applications of this technology use iron-based catalysts, which are known to carburize during reaction (1-5). Pre-nitriding of a fused iron catalyst has been reported to shift the molecular weight and alcohol content of the product distribution (6,7). Recent studies (8,9) indicate somewhat different selectivities for the nitrated catalysts, but confirm high activities and stability of nitrogen for a variety of catalyst and reaction conditions.

The structures and magnetic properties of the nitride phases have been investigated by various authors using several techniques, including XRD (10), LEED (11), Auger (12) and Mössbauer spectroscopy (13,14,15). Three nitride phases have been differentiated:  $\gamma$ -Fe<sub>4</sub>N,  $\epsilon$ -Fe<sub>x</sub>N (2 < x < 3), and  $\zeta$ -Fe<sub>2</sub>N. The phase diagram has been presented by Ertl *et al* (12). As the nitrogen content increases, the structure changes from BCC ( $\alpha$ -Fe), to FCC ( $\gamma$ -Fe<sub>4</sub>N), to HCP ( $\epsilon$ -Fe<sub>x</sub>N), to orthorhombic ( $\zeta$ -Fe<sub>2</sub>N). Mössbauer spectroscopy is particularly effective in differentiating the various iron nitrides (14,15).

In this work, we have used Mössbauer spectroscopy and transient mass spectrometric analysis to examine the stability, surface chemistry, and catalytic behavior of the three iron nitrides. We have found that at typical reaction temperatures, the pure nitride phases are unstable in both H<sub>2</sub> and synthesis gas, but in synthesis gas much nitrogen can be retained in the working catalyst in a carbonitride phase. We have continued this work by examining the nature of the surface before and during reaction in synthesis gas. Transient measurements show that surface nitrogen species are more reactive toward hydrogen than surface carbon species, and thus nitrogen is quickly lost from the surface during the first minutes of reaction. The high reactivity of nitrogen also suggests that a continuous supply of nitrogen from a reactant could lead to synthesis of nitrogen-containing compounds. The patent literature and our preliminary experiments confirm production of acetonitrile when NH<sub>3</sub> is added to synthesis gas at 700 K. Our findings also indicate that the use of catalysts with very small iron particles can affect the stability during reaction.

### EXPERIMENTAL

Preparation of the unsupported nitride powders was accomplished by reducing iron oxide at 325-400 C in flowing UHP hydrogen. The reduced iron powder (a compressed wafer in the Mössbauer apparatus, and a packed bed for the transient mass spec apparatus) was nitrated in a flowing mixture of ammonia and hydrogen for about 4 hours to produce the catalyst product. The nitrogen content was controlled by either altering the gas phase ammonia composition or varying the reaction temperature. Nitrogen content was checked by integrating the

mass spectrometer signal for  $\text{NH}_3$  when the nitride was reduced in hydrogen. Nitride phases were also identified by their Mössbauer spectra or XRD patterns.

The  $^{57}\text{Fe}$  Mössbauer spectra were recorded on a Nuclear Data multichannel analyzer from an Austin Science S-600 spectrometer. Both constant acceleration and constant velocity (transient) modes were used. All Mössbauer spectra isomer shift parameters are referenced to a  $25\mu\text{m}$  NBS Fe foil. The *in situ* Mössbauer cell supports a mechanically compressed sample wafer, allowing Mössbauer effect investigation of changes in the bulk sample during nitriding, denitriding, carburization, and synthesis reaction.

Details of reaction kinetics are studied by mass spectrometry. The apparatus used for this portion of the work was specifically designed for transient experiments. Combinations of reactant feed gases can be stepped or pulsed to the reactor. The effluent of the reactor is continuously measured by an Extranuclear EMBA II quadrupole mass spectrometer with a supersonic nozzle molecular beam inlet and phase sensitive detection. The spectrometer is controlled and monitored by a Digital MINC 11 microcomputer to facilitate the high speed gas analysis required for transient experiments.

## RESULTS AND DISCUSSION

The Mössbauer spectral variations with changing nitrogen content are depicted in Figure 1, with  $\alpha\text{-Fe}$  included for comparison. The  $\zeta\text{-Fe}_2\text{N}$  phase can be made at a variety of temperatures, but is most easily prepared at  $400^\circ\text{C}$  with 100% ammonia and identified by the narrowly split quadrupole doublet of Figure 1A. The  $\epsilon\text{-Fe}_x\text{N}$  phase is only prepared in a narrow concentration range of  $90 \pm 5\%$   $\text{NH}_3$ . Variation of the temperature changes the stoichiometry ( $2 < x < 3$ ) such that decreasing nitrogen content increases the species with hyperfine splitting of about 200kOe at the expense of the central quadrupole doublet (Spectra 1B-E). Slight changes in concentration also alter the stoichiometry of the  $\epsilon\text{-Fe}_x\text{N}$  phase (Figure 1F). The  $\gamma\text{-Fe}_4\text{N}$  phase is formed at lower ammonia concentrations (75%  $\text{NH}_3$ ) at  $325^\circ\text{C}$ , and is easily identified by its characteristic 8 line spectrum with its rightmost line at higher velocity than that of  $\alpha\text{-Fe}$  (Figure 1G).

The constant velocity capability of the Mössbauer drive allows *in situ* inspection of the nitriding process by following the growth or loss of transmitted intensity at a fixed velocity during the process. Figure 2 presents the loss (increase in transmission) and subsequent return of the central quadrupole doublet during denitriding and renitriding of  $\zeta\text{-Fe}_2\text{N}$ , observable by following the velocity indicated in the constant acceleration spectrum. The denitriding kinetics at  $325^\circ\text{C}$  are very rapid, converting the  $\zeta$  nitride to  $\alpha$  iron in seconds. On the other hand, the nitriding to the orthorhombic phase is relatively slow. During nitriding the nitrogen entering the lattice promotes a structural change from the relatively open bcc structure to the more dense orthorhombic arrangement which has considerably lower diffusivity of nitrogen. Ninety percent of the nitrogen appears to have entered the sample within 40 minutes of starting the nitriding.

Figure 3 shows the effect of gas phase composition on the rate of orthorhombic phase disappearance from  $\zeta\text{-Fe}_2\text{N}$ , as followed by constant velocity measurement of the central doublet at 0.5 mm/sec in the Mössbauer spectrum. The effect of pure hydrogen at  $325^\circ\text{C}$  has already been seen in Figure 2. At  $250^\circ\text{C}$ , the nitrogen loss remains rapid (Figure 3A). Removal of nitrogen in the form of  $\text{N}_2$  in He is very much slower (Figure 3B). The phase disappearance is very fast in  $3\text{H}_2/\text{CO}$  as well, (Figure 3C) but in this case does not reflect fast loss of substantial nitride nitrogen to ammonia in the gas phase. Constant acceleration spectra taken

after 20 minutes of exposure to  $3\text{H}_2/\text{CO}$  show that the initial contact with syngas first removes nitrogen from the lattice to form an  $\epsilon$  nitride, which has small contribution at the 0.5 mm/s velocity. Further reaction in synthesis gas then produces carbonitrides. Carburization in pure CO produces only a gradual structural change (Figure 3D). The final phase, as confirmed by the constant acceleration spectrum, is a very broad doublet which has little definition (less even than the spectrum in Figure 1D).

Investigation of the mechanism of nitride decomposition in hydrogen can be studied by mass spectrometry. In addition, surface species present during the nitriding process in ammonia can be identified by decomposition in deuterium. Figure 4 shows the decomposition of a  $\zeta\text{-Fe}_2\text{N}$  in deuterium into the deuterio-ammonias at 250°C. The  $\zeta\text{-Fe}_2\text{N}$  nitride was prepared in  $\text{NH}_3$  at 400°C, then cooled to 250°C in  $\text{NH}_3$  and the reactor then purged with argon for 10 minutes. The nitride and surface species are stable in argon at 250°C. The decomposition in  $\text{D}_2$  occurs quickly, as predicted from the Mössbauer results in Figure 2. From the shape of the  $\text{ND}_3$  curve, which is the decomposition product of the nitride nitrogen, it is clear that a slow activation is taking place. Modelling of this phenomenon indicates that a surface competition between the amount of adsorbed hydrogen (or in the case of Figure 4, adsorbed deuterium) and a nitrogen surface species can successfully simulate the results. Bulk nitride is converted to this nitrogen surface species.

Also apparent in Figure 4 are the mixed ammonias with hydrogen contributions. The presence of  $\text{NH}_x\text{D}_{3-x}$  in the effluent shows clearly that the fresh surface retains some hydrogen. The appearance of  $\text{NH}_3$  first does not indicate that  $x = 3$ , but is the result of chromatographic isotopic exchange at the leading edge of the deuterium pulse. This hydrogen most probably exists as a stable  $\text{NH}_x$  surface species left over from the nitriding procedure in  $\text{NH}_3$ . It will be seen that this  $\text{NH}_x$  species is very reactive and is removed in synthesis gas.

The deuterium experiment and the Mössbauer studies show that some of the nitrogen in the pure nitrides is very labile. The transient mass spectrometric approach allows us to measure relative surface reactivities directly. Figure 5 shows the response of a freshly prepared and He-purged surface to 3/1  $\text{H}_2/\text{CO}$ . The curves show clearly that surface hydrogen reacts preferentially with surface nitrogen rather than surface carbon. About 1.6 monolayer's worth of ammonia comes off before methane production starts. The  $\text{CO}_2$  curve shows that carbon is being deposited on the surface by the Boudouard reaction while hydrogen is being scavenged by the surface  $\text{NH}_x$  groups. The availability of surface species changes dramatically after five minutes on stream. Figure 6 shows the response of the reacting system to a short He pulse followed by a switch to hydrogen. The burst of methane is characteristic of excess surface carbon. Ammonia evolves only slowly from the catalyst. Because of the high reactivity of surface nitrogen species just demonstrated above, we take this result to indicate very low nitrogen content on the the surface of the working catalyst. The high reactivity of surface nitrogen with hydrogen can be delayed, but not suppressed, by the presence of excess surface carbon. If the surface of a fresh nitride is precarburized in CO and then exposed to synthesis gas, as shown in Figure 7, the surface carbon layer delays any activity for a short induction time, but then nitrogen is released as ammonia before carbon can react to methane. The surface  $\text{NH}_x$  species is therefore stable in helium or pure carbon monoxide at 250°C.

We have also begun studying iron nitrides supported on carbon. A small particle 5% iron on Carbolac-1, which is a high surface area (1000  $\text{m}^2/\text{g}$ ) carbon support, was prepared and reduced in hydrogen for 16 hours at 400°C. The room temperature Mössbauer spectrum of this reduced catalyst is shown in Figure 8a. The broad singlet at 0.0 mm/sec may be ascribed to superparamagnetic  $\text{Fe}^0$ . The typical six line pattern collapses to a superparamagnetic

singlet when the relaxation time is short compared to the lifetime of the excited state of the nucleus. We may therefore conclude that our iron crystallites are small. The asymmetric nature of this spectrum is due to the contribution of  $\text{Fe}^{2+}$  at 0.8 mm/sec, which arises from incomplete reduction of the passivated iron. Extensive (21 hrs) exposure to UHP He that was further purified in oxygen traps resulted in the spectrum of Figure 8b. The increased absorbance of the  $\text{Fe}^{2+}$  peak indicates that the catalyst is passivated in helium with oxygen concentrations on the order of 1 ppb. This catalyst was nitrided in pure  $\text{NH}_3$  at  $400^\circ\text{C}$  for 8 hours to produce the  $\zeta\text{-Fe}_2\text{N}$  phase, indicated by the doublet seen in Figure 8c. Figure 8d shows the result of exposure of this catalyst to 3/1  $\text{H}_2/\text{CO}$  at  $250^\circ\text{C}$  for 20 hours. This spectrum has the same general appearance of other bulk nitrided samples following FTS and indicates a complex mixture of nitride, carbide and carbonitride phases. Rereduction of this sample resulted in the spectrum shown in Figure 8e, showing major contributions (84%) from a bulk Fe metal pattern. Thus, the iron crystallites have sintered during the nitriding-reaction-reduction process. In previous experiments, we have shown that small particle  $\text{Fe}_4\text{N}$  on carbon has stable activity during Fischer-Tropsch synthesis. Our results here suggest that maintaining the small size of the particles is important to maintaining the stability of the nitride catalyst. The point in the process at which particle growth occurs is currently under investigation.

#### REFERENCES

1. Amelse, J.A., Butt, J.B. and Schwartz, L.H., *J. Phys. Chem.*, **82** (5), 558 (1978).
2. Anderson, R.B. and Hofer, L.J.E., in *Catalysis, Vol IV.* (Emmett, P.H., ed.), Reinhold, New York (1956).
3. Anderson, R.B., *The Fischer-Tropsch Synthesis* Academic Press, Orlando (1984).
4. Niemantsverdriet, J.W., van der Kraan, A.M., van Dijk, W.L. and van der Baan, J. *Phys. Chem.*, **84**, 3863 (1980).
5. Ott, G.L., Fleisch, T. and Delgass, W.N. *J. Cat.*, **65**, 253 (1980).
6. Anderson, R.B., *Cat. Rev.-Sci. Eng.*, **21** 53 (1980).
7. Borghard, W.G. and Bennett, C.O., *I&EC Prod. Res. & Dev.*, **18** 18 (1979).
8. Yeh, E.B., Jaggi, N.K., Butt, J.B., and Schwartz, L.H., *J. Catal.* **91**, 231 (1985).
9. Yeh, E.B., Schwartz, L.H., and Butt, J.B., *J. Catal.* **91**, 241 (1985).
10. Jack, K.H., *Acta Crystallogr.*, **5**, 404 (1952).
11. Grunze, M., Bozso, F., Ertl, G. and Weiss, M., *Appl. Surf. Sci.*, **1**, 241 (1978).
12. Ertl, G., Huber, M., and Thiele, N., *Z. Naturforsch. A.*, **34**, 30 (1979).
13. Shirane, G., Takei, W.J. and Ruby, S.L., *Phys. Rev.*, **126** (1), 49 (1962).
14. Bainbridge, J., Channing, D.A., Whitler, W.H., and Pendelburg, R.E., *J. Phys. Chem. Solid*, **34**, 1579 (1973).
15. Chen, G.M., Jaggi, N.K., Butt, J.B., Yeh, E.B. and Schwartz, L.H., *J. Phys. Chem.*, **87**, 5326 (1983).

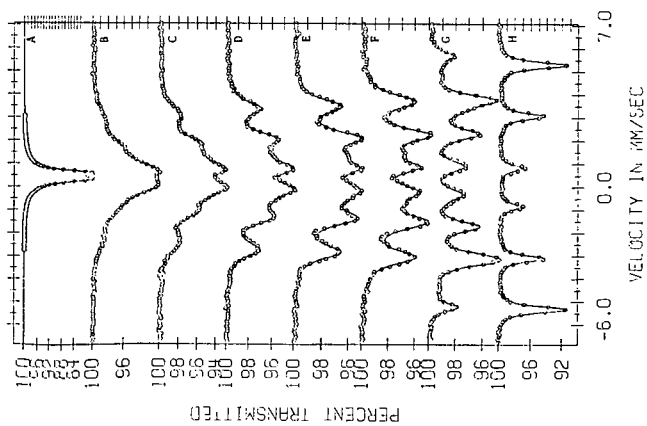


Figure 1. - Room Temperature Mössbauer spectra of iron nitrides.  
 A)  $\zeta$ -Fe<sub>3</sub>N; B-F)  $\epsilon$ -Fe<sub>2</sub>N prepared by exposure of  $\alpha$ -Fe to 91% NH<sub>3</sub>, 9% H<sub>2</sub> at 400°C (B), 325°C (C), 280°C (D), 250°C (E) and to 89% NH<sub>3</sub>, 11% H<sub>2</sub> at 400°C (F); G)  $\gamma$ -Fe<sub>2</sub>N; H)  $\alpha$ -Fe

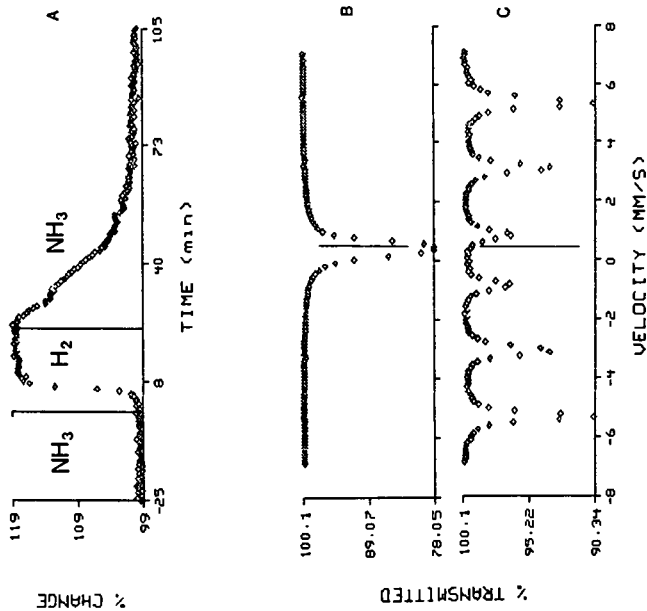


Figure 2. - Mössbauer spectra of  $\zeta$ -Fe<sub>2</sub>N during nitriding and denitriding.  
 A) Constant velocity spectrum, at the velocity indicated by the lines in spectra B) and C), taken at 325°C during a switch from NH<sub>3</sub> to H<sub>2</sub> and back to NH<sub>3</sub>. B) Spectra of the initial and final  $\zeta$ -Fe<sub>2</sub>N at 25°C. C) 25°C spectrum of  $\alpha$ -Fe after denitriding.

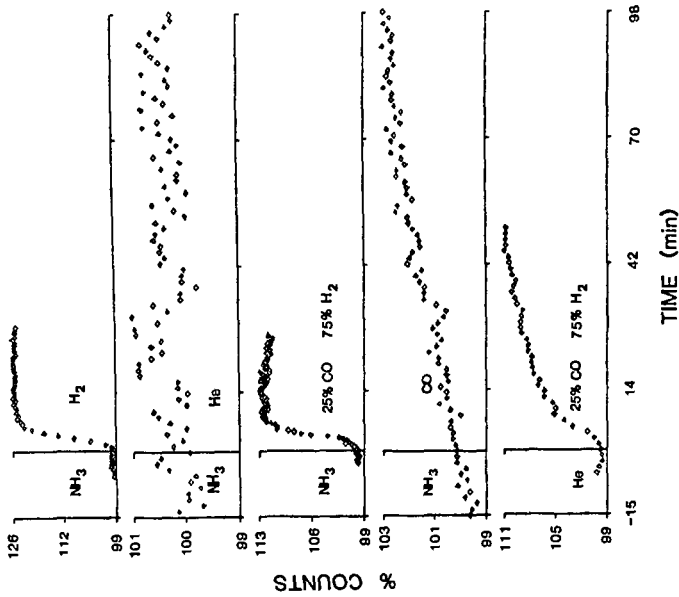


Figure 3. - *In situ* analysis of  $\zeta\text{-Fe}_2\text{N}$  stability at 250°C.

- step change to  $\text{H}_2$  from  $\text{NH}_3$
- step change to He from  $\text{NH}_3$
- step change to  $3\text{H}_2/\text{CO}$  from  $\text{NH}_3$
- step change to CO from  $\text{NH}_3$
- step change to  $3\text{H}_2/\text{CO}$  from  $\text{NH}_3$  over pre-oxidized  $\zeta\text{-Fe}_2\text{N}$

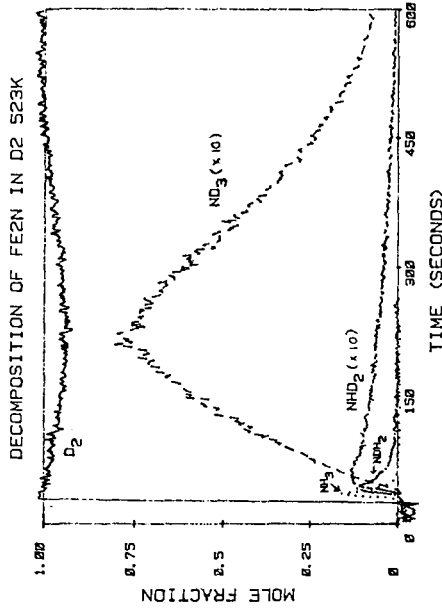


Figure 4. - Decomposition of  $\zeta\text{-Fe}_2\text{N}$  in deuterium at 250°C after purging in argon.

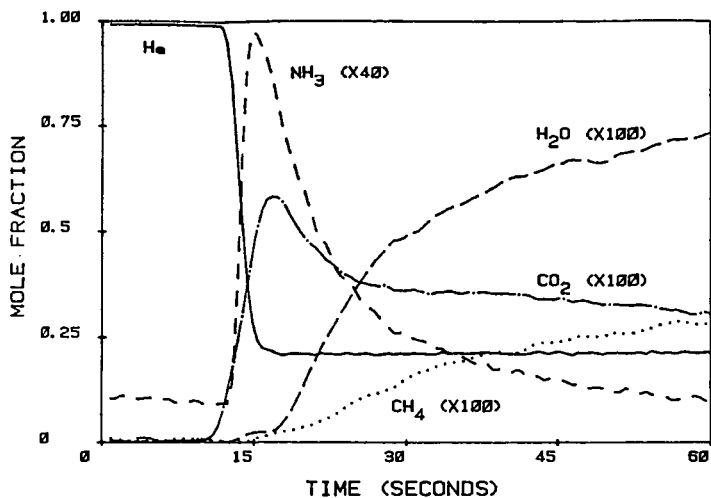


Figure 5. - Step change from helium to 3 H<sub>2</sub>/1 CO/1 He over an  $\epsilon$  nitride at 250°C.

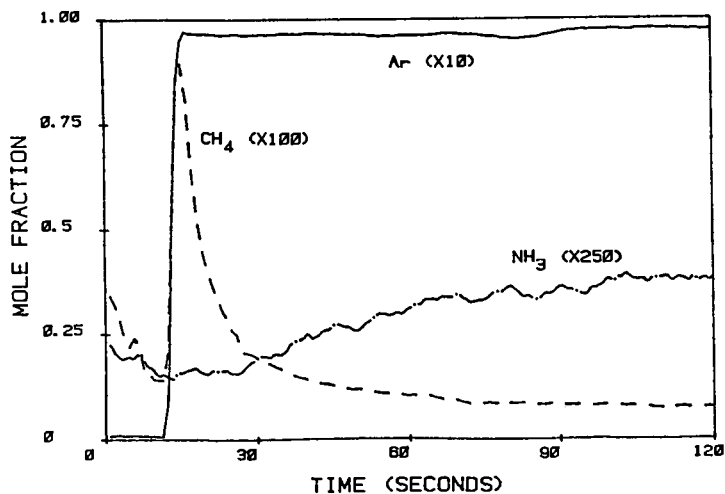


Figure 6. - Step from helium to 10 H<sub>2</sub>/Ar over an  $\epsilon$  nitride after 5 min. of FT synthesis in 3/1 H<sub>2</sub>/CO at 250°C.

MOSSBAUER SPECTRA 5MTX IRON ON CARBOLAC

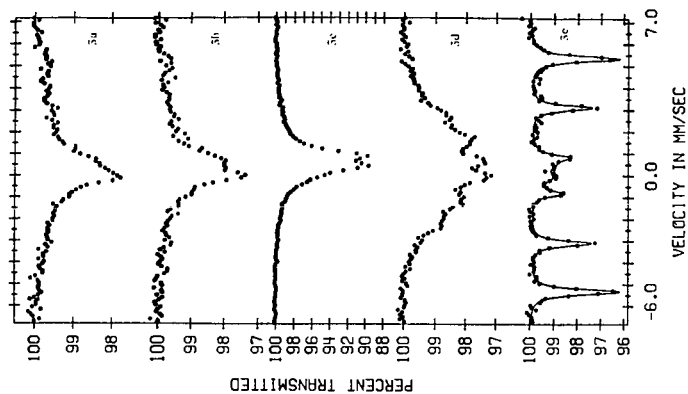


Figure 8. - Mossbauer spectra of 4.5 wt% Fe supported on carbolac.  
 a) Reduced in  $H_2$  at  $400^\circ C$  for 16 hrs.  
 b) Exposed to He at RT for 21 hrs.  
 c) Nitrided to  $\zeta-Fe_3N$  using 100  $NH_3$  at  $400^\circ C$  for 8 hrs.  
 d) Post - FTS at  $250^\circ C$  for 20 hrs.  
 e) Reduced in  $H_2$  at  $400^\circ C$  for 4 hrs.

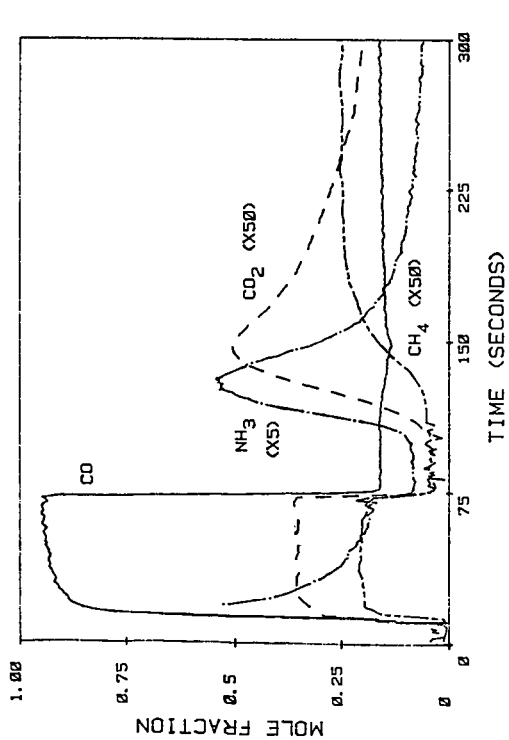


Figure 7. - Pretreatment of a  $\zeta-Fe_3N$  catalyst in 1 min. of CO followed by 3/1  $H_2/CO$  at  $250^\circ C$ .

## THE SURFACE CHEMISTRY OF IRON FISCHER-TROPSCH CATALYSTS

D. J. DWYER AND J. H. HARDENBURGH

Exxon Research and Engineering  
Corporate Research Science Laboratory  
Route 22 East  
Annandale NJ. 08801

### INTRODUCTION

The indirect conversion of coal to liquid hydrocarbons via steam gasification followed by synthesis gas ( $\text{CO}/\text{H}_2$ ) chemistry has been the subject of intensive study for a number of decades. A key technological challenge facing researchers in this area is control over the product distribution during the hydrocarbon synthesis step. In the case of iron Fischer-Tropsch catalysts, it has long been known that the addition of alkali to the metal catalyst has a significant impact on the product distribution(1). Iron catalysts treated with alkali produce less methane more alkenes and higher molecular weight products. In spite of numerous investigations (2-9), the details of this promotional effect are not understood on a molecular level. To explore the role of alkali in the surface chemistry of iron catalysts, we have carried out a combined surface science and catalytic kinetic study of a model iron catalyst with and without surface alkali.

### EXPERIMENTAL

The experimental apparatus has been described elsewhere (10,11). It consists of a medium pressure microreactor coupled to a ultra-high vacuum system equipped to perform x-ray photoelectron spectroscopy. The microreactor was a small UHV compatible tube furnace with an internal volume of approximately 10 cc and gold plated walls for inertness. The catalysts used in the study were pressed into a gold mesh backing material which in turn was mounted on a gold sample boat. The boat and the sample could be shuttled back and forth between the high pressure reactor and the UHV surface analysis chamber via a special UHV manipulator.

The iron catalysts were prepared by reducing ultra-high purity iron oxide ( $\text{Fe}_2\text{O}_3$ ) in an external tube furnace. The reduction was carried out to completion at 675K, 1 atm  $\text{H}_2$  for 24 hours. The surface of this pyrophoric powder was then passivated for 2 hours in a 1%  $\text{O}_2$  in He mixture. The passivated iron powder was characterized by x-ray diffraction and only  $\alpha$ -iron was detected. XPS analysis of the same sample revealed only  $\text{Fe}_2\text{O}_3$  on the surface. These data indicate that the passivated iron powder consists of an iron core surrounded by a thin skin of iron oxide.

2.5 grams of the passivated powder was impregnated with .015 grams of  $\text{K}_2\text{CO}_3$  through a standard aqueous incipient wetness technique. The surface areas of the two samples (with and without) alkali were determined by the BET method. The potassium containing catalyst had a surface area of  $16 \text{ M}^2/\text{gram}$  and the untreated catalyst had a surface area of  $18 \text{ M}^2/\text{gram}$ . Assuming complete dispersion of the potassium and a surface site density on the iron of  $10^{15}/\text{cm}^2$ , the potassium coverage on the iron surface is approximately

1/3 of a monolayer.

## RESULTS AND DISCUSSIONS

A detailed report on the surface compositional changes that accompany pretreatment and activation of the iron catalysts has been reported elsewhere (10-11). The surface of the untreated iron catalyst consists primarily of iron in +3 oxidation state ( $\text{Fe}_2\text{O}_3$ ). Upon reduction ( $\text{H}_2$ , 2 atm, 625 K), the surface is converted to metallic iron. The metallic iron surface is, however, unstable under synthesis gas ( $\text{H}_2:\text{CO}$  3:1, 525 K, 6atm) and is slowly converted to iron carbide. Concomitant with the carbidization of the iron surface is a marked increase in the rate of catalytic reaction of CO to hydrocarbons. Steady state activity is reached after 3-4 hours under reaction conditions. The steady state product distribution of the unpromoted iron carbide surface consists primarily of methane and small linear alkanes. Two types of carbon species were identified on the surface of unpromoted material after reaction. A carbidic form of carbon that was reactive to  $\text{H}_2$  and was easily converted to methane. The second type of surface carbon was a coke-like or graphitic deposit that was very unreactive to  $\text{H}_2$ . This second type of carbon was found to dominate the surface and poison the reaction when the reaction was run at elevated temperatures.

The surface of the potassium treated catalyst after reduction consisted of a metallic iron with a strongly adsorbed potassium oxygen complex of approximately 1:1 stoichiometry. The stability of this complex is evident since it is formed by decomposition of the thermodynamically stable  $\text{K}_2\text{CO}_3$ . Upon exposure to synthesis gas the metallic iron is once again converted to iron carbide and a slow increase in reactivity accompanies this change in surface composition. The product distribution over the potassium treated catalyst is substantially different than that observed over the unpromoted surface. The methane yield is lower, the average molecular weight is higher and the product now consists primarily of linear alkenes. After reaction the surface is covered by layer of hydrocarbon which is best characterized as polymethylene.

It has been suggested in the literature that the role of surface alkali in this reaction is to facilitate the dissociation of CO on the surface (9). Presumably, the increased concentration of reactive carbon on the surface shifts the product distribution towards higher molecular weights by enhancing the chain building step in the reaction. However, the results of this study clearly show that the iron and iron carbide surfaces easily break the carbon-oxygen bond in CO. The unpromoted catalyst is saturated in carbon which is reactive towards hydrogen. Therefore, it does not seem reasonable that the role of surface alkali is to enhance CO dissociation. The simple and straight forward explanation of the results of this study is that originally proposed by Dry(2). Potassium addition increases the heat of adsorption of CO and weakens the adsorption of  $\text{H}_2$  which in turn changes the relative concentrations of CO and H on the surface of the catalyst under reaction conditions. Our results indicate that the unpromoted iron carbide is a very good hydrogenation catalyst producing primarily small alkanes. Little or no hydrocarbon fragments are observed on the surface after reaction. When potassium is added the overall hydrogenation activity of the surface drops. Larger alkanes dominate the product and there is an accumulation of hydrocarbon

fragments or intermediates on the surface. It appears that the unpromoted surface is too good a hydrogenation catalyst with a high hydrogen activity at the surface. The hydrocarbon intermediates which form on the surface are rapidly intercepted by surface hydrogen and terminated as small alkanes. When potassium is present the hydrogen activity at the surface is much lower, this allows the hydrocarbon intermediates to accumulate and polymerize on the surface and results in larger molecules which are alkenes and not alkanes.

#### REFERENCES.

1. F. Fischer and H. Tropsch, Ber. Deut. Chem. Ges. B59(1926) 830.
2. M.E. Dry, T. Shingles, L. J. Boshoff and G.J. Oosthuizen, J. Catalysis 15 (1969) 190.
3. J. Benziger and R. J. Madix, Surface Science 94 (1980) 119.
4. K. Subramanzam and M. R. A. Rao, J. Res. Inst. Catalysis Hokkaido 18 (1970) 124.
5. H. Kobel and W.K. Muller, Ber. Bunsenges Physik. Chem. 67 (1963) 212.
6. G. Broden, G. Gafner and H.P. Bonzel, Surface Science 84 (1979) 295.
7. S. R. Kelemen, A. Kaldor and D. J. Dwyer, Surface Science 121 (1982) 303.
8. J. E. Crowell, E. L. Garfunkel and G.A. Somorjai, Surface Science 121 (1982) 303.
9. H. P. Bonzel, Chem. Ing. Tech. 54 (1982) 908.
10. D. J. Dwyer and J. H. Hardenburgh, J. Catalysis 87 (1984) 66.
11. D. J. Dwyer and J. H. Hardenburgh, Appl. Surface Science 19 (1984) 14.

atmosphere. Product gases exiting the cell were analyzed by gas chromatography (temperature programmed Porapak Q column) utilizing a combination of thermal conductivity and flame ionization detection. Following evacuation of the reaction cell, samples could be transferred into the UHV chamber without exposure to air.

The materials characterized included high purity iron foils (Johnson Matthey), and commercially obtained  $\text{Fe}_3\text{O}_4$  and  $\text{Fe}_2\text{O}_3$  powders (Alfa Products). Oxide samples were mounted by pressing the powders into 48 mesh copper screen. All synthesis reactions were carried out over the  $\text{Fe}_2\text{O}_3$  powder, after first reducing the oxide in flowing hydrogen for 9 hours at  $400^\circ\text{C}$ . Hydrogen chemisorption measurements, using the method described by Amelse, et al. (12), yielded an uptake of  $21 \mu\text{mole H}_2/\text{g Fe}$  for the reduced powder. Specific reaction rates were calculated based on the hydrogen uptake, assuming two surface iron sites per adsorbed  $\text{H}_2$  molecule. Gases used in the sample reductions and synthesis reactions were dried by passage through a silica gel bed immersed in a dry ice/acetone bath. Oxygen impurities were removed by a 10%  $\text{MnO}/\text{SiO}_2$  trap which had previously been reduced in flowing hydrogen at  $350\text{--}400^\circ\text{C}$ . The 3:1  $\text{H}_2/\text{CO}$  synthesis mixture (Matheson) was obtained in an aluminum cylinder to minimize the formation of carbonyls. A silica gel trap heated to  $200^\circ\text{C}$  was used to remove any carbonyls present in the reactant stream.

## RESULTS

### Oxidized Iron Surfaces

The  $\text{Fe}(2p)$  XPS spectra characteristic of iron and the stoichiometric oxides are summarized in Figure 1. The metallic iron spectrum (Figure 1a) was measured for a foil sample after the surface had been cleaned by repetitive cycles of argon ion sputtering and annealing at  $450^\circ\text{C}$  in the vacuum chamber. The surfaces of the air-exposed oxide powders were invariably contaminated by adsorbed water, as evidenced by broadening on the high binding energy side of the  $\text{O}(1s)$  XPS peaks. In the case of the  $\text{Fe}_2\text{O}_3$  powder, mild heating in vacuum (1 hr at  $170^\circ\text{C}$ ) removed nearly all of this surface contamination, resulting in the spectrum shown in Figure 1c. The surface of the  $\text{Fe}_3\text{O}_4$  powder was at least partially oxidized to  $\text{Fe}_2\text{O}_3$ , based on the  $\text{Fe}(2p)$  peak positions and satellite structure measured for as-prepared samples. Using the spectrum fitting procedure described below, we observed that brief (<2 min) argon ion sputtering of iron oxide surfaces results in the reduction of  $\text{Fe(III)}$  to  $\text{Fe(II)}$ , while prolonged sputtering leads to the formation of a significant metallic iron phase. In either case, this surface reduction is accompanied by a decrease in the ratio of the oxygen to iron XPS intensities. The  $\text{Fe}_3\text{O}_4$  spectrum (Figure 1d) was obtained for a powder sample after brief argon ion sputtering, followed by heating for 5 hours at  $350^\circ\text{C}$  in vacuum. During this sample heating, the  $\text{O}(1s)/\text{Fe}(2p_{3/2})$  intensity ratio increased steadily and then leveled off, signaling a gradual re-oxidation of the sputtered surface.

In a recent review of oxide photoemission studies, Wandelt (13) observed that the  $\text{Fe}(2p)$  XPS spectrum of  $\text{Fe}_3\text{O}_4$  is simply a weighted average of the spectra for  $\text{Fe}_2\text{O}_3$  ( $\text{Fe(III)}$ ) and  $\text{Fe}_x\text{O}$  (primarily  $\text{Fe(II)}$ ). This is illustrated by the  $\text{Fe(II)}$  spectrum in Figure 1b, which was obtained by subtracting out the  $\text{Fe(III)}$  contribution to the  $\text{Fe}_3\text{O}_4$  spectrum (assuming an  $\text{Fe(III)}$  to  $\text{Fe(II)}$  area ratio of 2:1). The resulting  $\text{Fe(II)}$  peak positions and satellite structure are in excellent agreement with XPS results reported for  $\text{Fe}_x\text{O}$  (13,14).

Spectra representing the individual oxidation states of iron (Figure 1a,b,c) can be used to analyze data obtained for partially oxidized surfaces, as illustrated in Figure 2. The points in this figure indicate data measured for an iron foil after brief exposures to  $1 \times 10^{-6}$  torr of oxygen at  $400^\circ\text{C}$ . The solid curves through these points indicate linear combinations of the spectra representing the individual iron oxidation states. Coefficients for these linear combinations were determined using the usual least squares minimization criteria. The individual contributions of each oxidation state to the fitted spectra are also indicated in Figure 2. This procedure allows the compositions of partially oxidized surfaces to be approximated in terms of the area contributions of each oxidation state to the total XPS spectrum. Area contributions to the spectra in Figures 2a and 2b are 78% Fe / 7% Fe(II) / 15% Fe(III), and 23% Fe / 29% Fe(II) / 48% Fe(III), respectively.

#### Carbided Iron Surfaces

Iron carbides were prepared by treating reduced powder samples either with ethylene or a 3:1  $\text{H}_2/\text{CO}$  mixture at  $250\text{--}275^\circ\text{C}$ . Analysis of these samples by Mössbauer spectroscopy indicated that the powders were fully carburized and consisted primarily of  $\chi\text{-Fe}_5\text{C}_2$ . XPS results for the carbide powders did not depend on the carburization medium employed, and we therefore limit discussion in this section to samples carbided under normal synthesis conditions ( $250^\circ\text{C}$ , 1 atm, 3:1  $\text{H}_2/\text{CO}$ ).

The catalytic behavior of the initially reduced powder is illustrated in Figure 3. The turnover frequency for methane formation increased steadily during the first 4 hours of synthesis and then remained nearly constant at  $\sim .0035$  molecules/site sec for times in excess of 20 hours. The steady state turnover frequency compares well with values in the range of .003 to .007 molecules/site sec reported by Amelse, et al. (12) for silica supported iron under similar reaction conditions. The steady state CO conversion level over the iron powder catalyst was 0.6%, based on integration of the  $\text{C}_1$  to  $\text{C}_5$  hydrocarbon products. Analysis of the hydrocarbon product distribution by the Schulz-Flory model yielded a chain growth parameter  $\alpha = 0.48$ .

XPS results obtained for the iron powder in the reduced and fully carburized states are summarized in Figure 4. The reduced catalyst exhibited an  $\text{Fe}(2p_{3/2})$  binding energy of 707.0 eV, and a shift to 707.3 eV was observed following exposure to synthesis conditions for 30 hours. Dwyer and Hardenbergh (15) reported a similar shift upon carburization of unsupported iron during low conversion synthesis at 7 atm. In addition to small increases in the iron core level binding energies, the metal and carbide phases are distinguished by differences in the iron Auger line shape, as illustrated in Figure 4. The most pronounced difference in line shape occurs for the  $\text{Fe}(\text{LMV})$  Auger transition, in the kinetic energy range from 610 to 660 eV. When Al  $\text{K}\alpha$  x-rays are used, this region also includes the  $\text{Fe}(2s)$  core level transition at a kinetic energy of ca. 639 eV.

Since the  $\text{Fe}(2p_{3/2})$  peaks of metallic iron and  $\chi\text{-Fe}_5\text{C}_2$  are nearly identical in shape and differ in position by only 0.3 eV, changes in the iron Auger spectrum provide a more useful method for characterizing mixtures of these phases. This is demonstrated by the results in Figure 5, which were obtained for a reduced powder sample after exposure to synthesis conditions for periods of 20 and 100 minutes. The Auger spectra in this figure were fit with linear combinations of the metal and carbide spectra (Figure 4), using the

least squares method described earlier. Area contributions of the carbide phase to the iron Auger spectra were 36% and 48% after synthesis for 20 and 100 minutes, respectively. The C(1s) spectra in Figure 5 illustrate the utility of XPS in characterizing the carbon adlayer which develops on catalyst surfaces during the Fischer-Tropsch synthesis. Krebs, et al. (9) have shown that the initial increase in activity observed during synthesis over iron foils is associated with the formation of surface "carbide" carbon, corresponding to the low binding energy (283.2 eV) C(1s) peaks in Figure 5. The high binding energy (285.3 eV) peaks in these spectra indicate the presence of graphitic surface carbon, which is associated with the deactivation of iron synthesis catalysts.

#### CONCLUSIONS

Analysis of Fe(2p) XPS and iron Auger spectra, combined with C(1s) XPS measurements, provides a valuable technique for studying the compositional behavior of Fischer-Tropsch catalysts. The extent of catalyst oxidation during synthesis at high conversions may be estimated in terms of the area contribution of oxide phases to the Fe(2p) spectrum. Similarities between the metal and carbide core level spectra are likely to complicate the determination of these phases when oxides are present. Analysis of the metal and carbide contributions to the iron Auger spectrum provides an alternate method for monitoring surface carbide formation during low conversion synthesis. The "surface compositions" obtained in this manner are at best semi-quantitative, since the contribution of a particular phase to the XPS or Auger spectrum will depend on both the amount and distribution of that phase within the detected volume. In spite of this, the spectrum fitting technique should prove to be useful in characterizing the time and conversion dependent nature of the active catalyst surface.

#### REFERENCES

- ( 1 ) J.A. Amelse, J.B. Butt, and L.H. Schwartz, *J. Phys. Chem.*, 82 , 558 (1978).
- ( 2 ) G.B. Raupp and W.N. Delgass, *J. Catalysis*, 58 , 348 (1979).
- ( 3 ) K.M. Sancier, W.E. Isakson, and H. Wise, *Adv. Chem. Ser.* 178 , 129 (1979).
- ( 4 ) J.W. Niemantsverdriet, A.M. van der Kraan, W.L. van Dijk, and H.S. van der Baan, *J. Phys. Chem.*, 84 , 3363 (1980).
- ( 5 ) G.B. Raupp and W.N. Delgass, *J. Catalysis*, 58 , 361 (1979).
- ( 6 ) H. Matsumoto, *J. Catalysis*, 86 , 201 (1984).
- ( 7 ) J.F. Shultz, W.K. Hall, B. Seligman, and R.B. Anderson, *J. Amer. Chem. Soc.*, 77 , 213 (1955).
- ( 8 ) R.B. Anderson, L.J.E. Hofer, E.M. Cohn, and B. Seligman, *J. Amer. Chem. Soc.*, 73 , 944 (1951).
- ( 9 ) H.J. Krebs, H.P. Bonzel, and G. Gafner, *Surf. Sci.*, 88 , 269 (1979).
- (10) H.P. Bonzel and H.J. Krebs, *Surf. Sci.*, 91 , 499 (1980).
- (11) H.J. Krebs and H.P. Bonzel, *Surf. Sci.*, 99 , 570 (1980).
- (12) J.A. Amelse, L.H. Schwartz, and J.B. Butt, *J. Catalysis*, 72 , 95 (1981).
- (13) K. Wandelt, *Surf. Sci. Reports*, 2 , 1 (1982).
- (14) M. Oku and K. Hirokawa, *J. Appl. Phys.*, 50 , 6303 (1979).
- (15) D.J. Dwyer and J.H. Hardenbergh, *J. Catalysis*, 87 , 66 (1984).

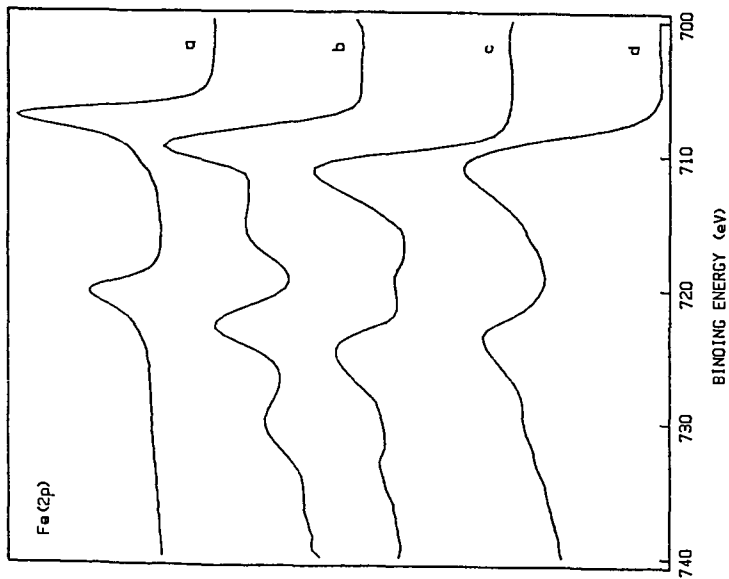


Figure 1. Fe(2p) XPS spectra of metallic iron and iron oxides. (a) clean foil (b) Fe(II) contribution to Fe<sub>3</sub>O<sub>4</sub> spectrum (c) Fe<sub>2</sub>O<sub>3</sub> (d) Fe<sub>3</sub>O<sub>4</sub>.

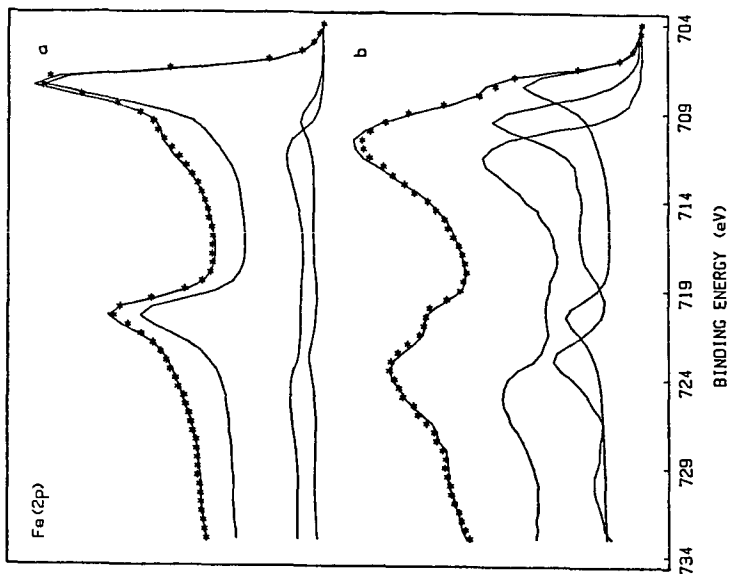


Figure 2. Examples of Fe(2p) spectrum fitting for partially oxidized iron foil. (a) 170 L O<sub>2</sub> (b) 670 L O<sub>2</sub> at 400°C.

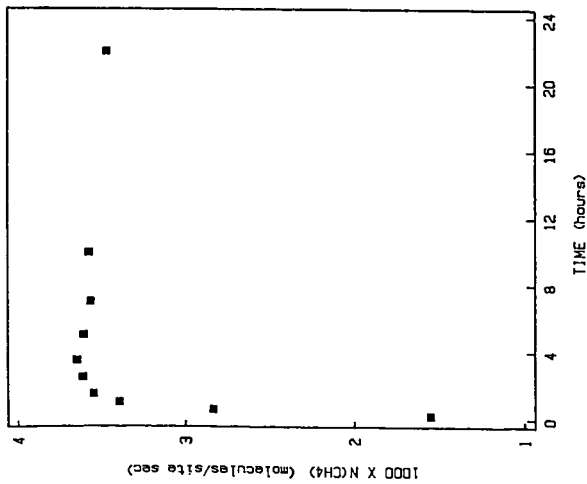
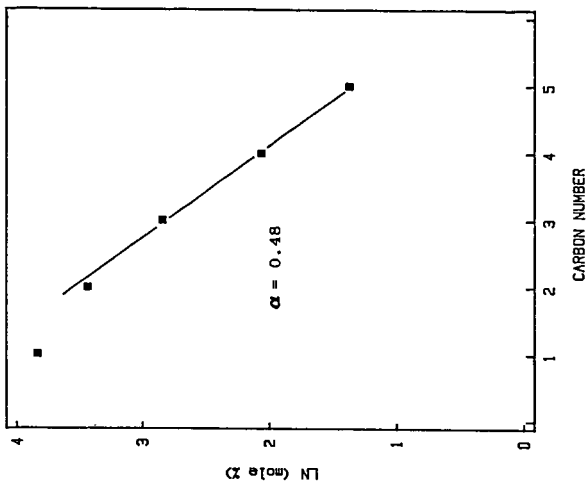


Figure 3. Methane turnover frequency versus time and steady state Schulz-Flory plot for synthesis over unsupported iron powder (250°C, 1 atm, 3:1 H<sub>2</sub>/CO).

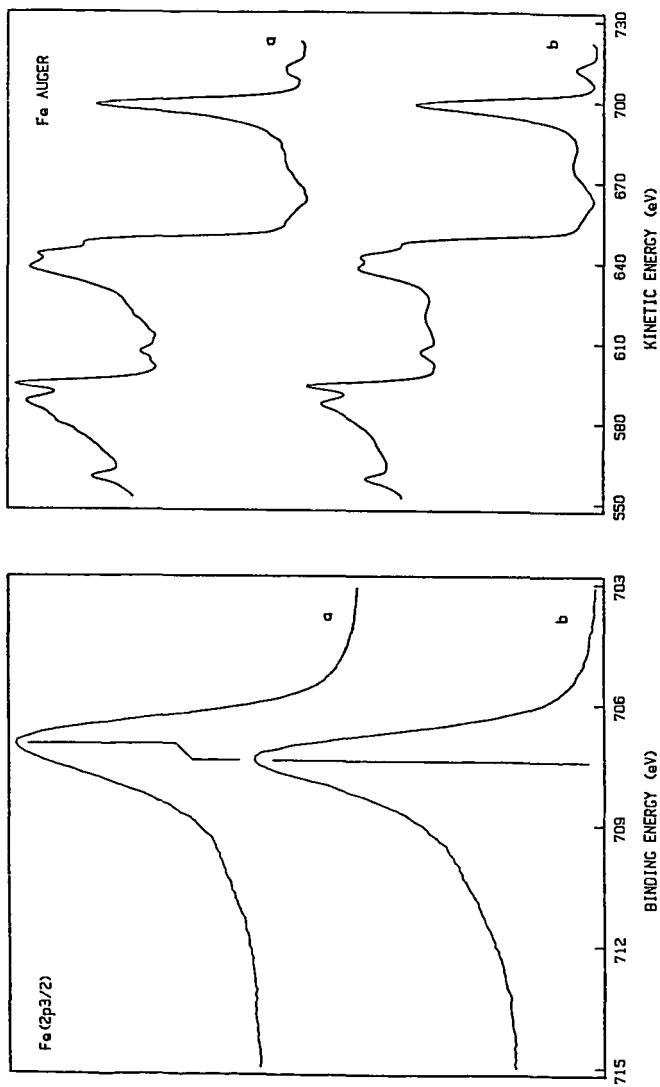


Figure 4. Fe(2p<sub>3/2</sub>) XPS and Fe Auger spectra of unsupported iron powder. (a) after reduction in 1 atm H<sub>2</sub> at 400°C (b) after hydrocarbon synthesis for 30 hr in 1 atm 3:1 H<sub>2</sub>/CO at 250°C.

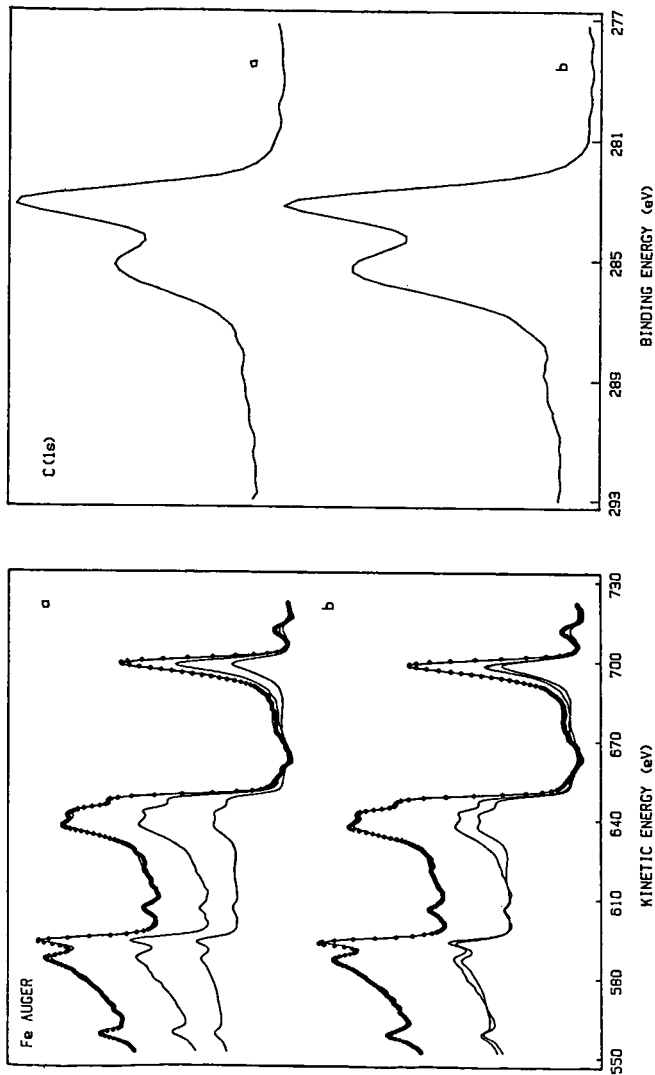


Figure 5. Fe Auger and C(1s) XPS spectra of unsupported iron powder after hydrocarbon synthesis for (a) 20 min (b) 100 min. Fe Auger spectra area contributions are: (a) 64% metal, 36% carbide (b) 52% metal, 48% carbide.

## XPS Characterization of Iron Fischer-Tropsch Catalysts

C. S. Kuivila, P. C. Stair, and J. B. Butt

Department of Chemical Engineering and Department of Chemistry  
Northwestern University, Evanston, Illinois 60201

### INTRODUCTION

The carburization of iron catalysts during the Fischer-Tropsch synthesis has received considerable attention, with techniques such as Mössbauer spectroscopy, x-ray diffraction, and thermomagnetic analysis being used to identify the bulk iron phases which are formed (1-4). Based on a recent Mössbauer study of unsupported iron (4), it is fairly well established that the  $\epsilon$ -Fe<sub>2</sub>C and  $\chi$ -Fe<sub>5</sub>C<sub>2</sub> carbides form at normal synthesis temperatures (ca. 250°C), while substantial amounts of cementite ( $\theta$ -Fe<sub>3</sub>C) are formed at temperatures above 350°C. Studies of both supported (1,5) and unsupported (4,6) iron have shown that the synthesis activity of an initially reduced catalyst is low, and increases to a maximum as carburization proceeds. Earlier work done at the Bureau of Mines (7) also suggests that controlled pre-carburization of fused iron catalysts at lower temperatures may improve long-term activity maintenance during the synthesis.

Although recent carburization studies have typically involved CO conversion levels in the range of a few percent or less, it is clear from work done at the Bureau of Mines (7,8) that higher conversion levels lead to significant oxidation of iron catalysts to Fe<sub>3</sub>O<sub>4</sub>. The working catalyst can thus consist of a mixture of metallic, carbide, and oxide phases, the relative amounts depending on catalyst pretreatment, synthesis conditions, and time on stream. A result of this complex behavior is that no clear picture exists regarding the nature of the catalytically active surface, or its dependence on the conditions employed in the synthesis. Much of the early work involving surface techniques (XPS/AES) in the study of CO hydrogenation over iron was carried out using foils or single crystals as model catalyst surfaces (9-11). Efforts in these studies focused on characterization of the carbon adlayer which developed on the metal surfaces during exposure to synthesis conditions.

In this paper, we address the XPS characterization of iron phases which occur on the surfaces of Fischer-Tropsch catalysts. Results obtained for single-phase metal, oxide, and carbide samples are presented. Methods for estimating the extent of carbide formation during low conversion synthesis, and the extent of catalyst oxidation at high conversions are also illustrated.

### EXPERIMENTAL

The XPS measurements were performed in an AEI ES200 ESCA spectrometer, equipped with a hemispherical electrostatic energy analyzer and aluminum-anode x-ray source. Electron binding energies were referenced to the Au(4f<sub>7/2</sub>) line of a gold foil at 84.0 eV. Samples were introduced into the system through a small volume (30 cc), differentially pumped reaction cell, attached directly to the vacuum chamber. The samples were mounted on a copper stage which could be heated resistively to 500°C, with temperature measurement by a chromel-alumel thermocouple junction. While in the cell, samples could be exposed to static or flowing gases at pressures up to one

In Situ Study of the Surface Interactions  
In Coal Liquefaction Catalysts

P.A. Montano

Dept. of Physics, West Virginia University, Morgantown, WV 26506

There is an increasing interest in the development of better catalysts for the hydrodenitrogenation (HDN) and hydrodesulfurization (HDS) of coal derived fuels and oil heavy residues. These synthetic feedstocks and heavier petroleum fractions contain a higher concentration of heteroatoms than light petroleum stocks and are much more difficult to process. Metal sulfides catalysts play a very important role in HDN and HDS processes as well as in direct coal liquefaction. There is concrete evidence of the direct role played by iron sulfides in direct coal liquefaction. We have investigated the surface reactions on iron sulfides, especially pyrrhotites using standard surface techniques, EXAFS and in situ Mossbauer spectroscopy. We find clear evidence of the involvement of the iron sulfides surfaces in the cleavage of oxygen bonds in coal and coal derived products. In HDN and HDS reactions, the role of the iron sulfides is less important than that of Mo-Co or Mo-Ni supported catalysts. We have performed a systematic in situ study of Ni-Mo supported on gamma alumina using x-ray absorption techniques as well as in situ Mossbauer spectroscopy. The HDN of quinoline was studied by both techniques between room temperature and 440°C at high hydrogen pressures. We find clear evidence of Ni association to Mo, there is also Ni in separated islands and a third phase of Ni interacting strongly with alumina and forming nickel-aluminate. When sulfidation takes place immediately after calcination two sulfide phases are identified, one associated with the MoS<sub>2</sub> islands on the support and the other, probably, with a non-stoichiometric nickel sulfide compound. Very small amounts of nickel aluminate are observable.

The HDS of dibenzothiophene was studied using a pure MoS<sub>2</sub> catalyst and a commercial Ni-Mo catalyst. The structure of the catalysts was investigated using x-ray absorption techniques. All the measurements were performed in situ between -195°C and 440°C. It was observed that the presence of nickel tends to stabilize the MoS<sub>2</sub> islands on the support; in the absence of nickel there is very clear evidence of irreversible sulfur loss.

The difference in catalytic activity between iron sulfides and Mo sulfides is related to the difference in crystallographic structures, which favors in the case of Mo a high dispersion of the catalyst on the support.

Work supported by the USDOE.